



# Twenty Years of Trials and Insights: Bridging Legacy and Next Generation in ParFlow and Land Surface Model Coupling

Chen Yang<sup>1\*</sup>, Aoqi Sun<sup>1</sup>, Shupeng Zhang<sup>1</sup>,  
Yongjiu Dai<sup>1</sup>, Stefan Kollet<sup>2,3</sup>, Reed Maxwell<sup>4</sup>

<sup>1</sup>School of Atmospheric Sciences, Sun Yat-sen University, Zhuhai, China

<sup>2</sup>Institute of Bio- and Geosciences (IBG-3, Agrosphere), Forschungszentrum Jülich (FZJ), Jülich, Germany

<sup>3</sup>Center for High-Performance Scientific Computing in Terrestrial Systems (HPSC TerrSys), Geoverbund ABC/J, Jülich, Germany

<sup>4</sup>Department of Civil and Environmental Engineering, The High Meadows Environmental Institute and the Integrated GroundWater Modeling Center, Princeton University, Princeton, USA

\*Corresponding to: yangch329@mail.sysu.edu.cn

## Abstract

Groundwater plays a vital role in terrestrial water and energy cycles, yet it remains oversimplified in most Earth system models (ESMs), limiting their ability to represent key land-atmosphere interactions, including evapotranspiration partitioning, drought propagation, and boundary layer development. The original coupling of ParFlow with the Common Land Model (CoLM) in 2005 not only demonstrated the feasibility of integrating physically based groundwater models into ESMs, but also revealed emergent behaviors—such as lateral moisture redistribution, along with the buffering effects that emerge from enhanced subsurface connectivity—that cannot be captured by traditional land surface models (LSMs). This study reviews key findings from two decades of ParFlow–land/atmosphere coupled modeling efforts, highlighting how groundwater–land–atmosphere interactions shape surface energy balance and hydrologic connectivity across three dimensions: upward feedbacks, downward influences, and the critical zone of coupling. Given the substantial advances in LSMs such as CoLM over the past two decades, a renewed recoupling effort is warranted to enhance our understanding of groundwater’s role across a broader range of Earth system processes. Preliminary efforts to recouple ParFlow with the updated water and energy modules of CoLM demonstrate improved performance when evaluated against reanalysis and observational data. To ensure long-term sustainability, we propose a modular and maintainable coupling framework addressing functional extensibility, data/code interoperability, and parallel computing needs, in which area, TerrSysMP2 has taken early steps and may be considered an initial forerunner. Finally, we summarize existing ParFlow-based coupled systems and highlight the need for a community-led model intercomparison project (PLCMP) to benchmark performance, evaluate process coupling under varied configurations, and foster cross-community collaboration.



42

## 43 1. Introduction

44 In 2005, a study titled "*Development of a Coupled Land Surface and Groundwater Model*"  
 45 was published in *Journal of Hydrometeorology* (Maxwell and Miller, 2005). It introduced the  
 46 coupling of ParFlow (Ashby and Falgout, 1996; Jones and Woodward, 2001) and the Common  
 47 Land Model (CLM) (Dai et al., 2003), and validated the framework using both synthetic and  
 48 real-world test cases. The study highlighted the role of groundwater in land surface processes  
 49 (Fan et al., 2019; Zeng et al., 2018; De Graaf and Stahl, 2022; Seuffert et al., 2002), particularly  
 50 lateral subsurface flow (Figure 1)—a component that was not explicitly represented in most  
 51 land surface models (LSMs) at the time. This work represented an early step toward  
 52 incorporating physically based groundwater dynamics into Earth system modeling frameworks.

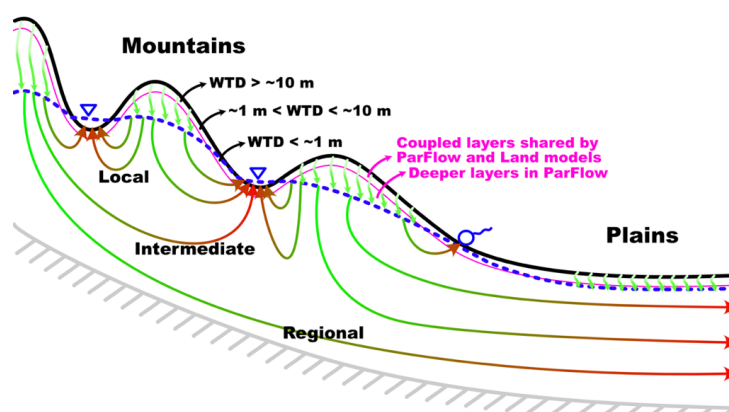
53 Since LSMs serve as the lower boundary in ESMs, this coupling provided a practical  
 54 pathway to incorporate groundwater dynamics into larger-scale Earth system frameworks.  
 55 Compared to earlier coupling attempts based on tightly integrated or proprietary platforms (Yeh  
 56 and Eltahir, 2005; Ivanov et al., 2004; York et al., 2002), this effort leveraged established  
 57 community models and an open design philosophy, facilitating broader applicability and long-  
 58 term adaptability. The resulting ParFlow-CLM model and other subsequent models coupled  
 59 with ParFlow have been applied in a range of hydrological and land-atmosphere studies  
 60 (Maxwell et al., 2007; Maxwell et al., 2011; Shrestha et al., 2014), contributing to improved  
 61 understanding of water and energy exchanges across subsurface, land surface, and  
 62 atmospheric domains (Rahman et al., 2015; Sulis et al., 2017; Keune et al., 2016; Forrester  
 63 and Maxwell, 2020). Even today, groundwater-land surface coupling remains underutilized in  
 64 many large-scale modeling frameworks, where groundwater models are often run offline with  
 65 limited interaction with land-atmosphere processes (De Graaf et al., 2017; Reinecke et al.,  
 66 2019; Verkaik et al., 2022).

67 The groundwater model, ParFlow, simulates fully 3D variably saturated subsurface flow  
 68 and overland flow by integrating Richards' equation with the shallow water equation in a unified  
 69 numerical framework (Kollet and Maxwell, 2006; Osei-Kuffuor et al., 2014; Maxwell, 2013).  
 70 Meanwhile, the Common Land Model (CLM, now CoLM) captures water and energy processes  
 71 from the canopy top to the bottom of the root zone. These two models were coupled through  
 72 the root zone (Figure 1), where net fluxes from CoLM after the interactions of infiltration and  
 73 evapotranspiration (ET) are treated as source/sink terms in ParFlow, while ParFlow returns soil  
 74 moisture and pressure head to CoLM to close the water and energy balance. Such a coupling  
 75 approach in terms of physics has been widely adopted by the following coupling works (Niu et  
 76 al., 2014; Fang et al., 2022; Maina et al., 2025).

77 After two decades of continuous development, LSMs such as CoLM have seen substantial  
 78 advancements in functionality, code architecture, data structures, I/O systems, pre-/post-  
 79 processing tools, and high-performance computing capabilities. ParFlow has undergone similar  
 80 progress on the hydrological modeling front. Although the original coupling between ParFlow



81 and CoLM was once considered sustainable, it is now increasingly inadequate in the face of  
 82 growing model complexity and volume. In light of these developments, we outline a sustainable  
 83 framework to support the next stage of ParFlow-LSM coupling development, with CoLM serving  
 84 as a primary example. This cross-disciplinary effort is expected to provide a robust platform for  
 85 the broader scientific community to efficiently apply coupled models, pursue advanced Earth  
 86 system inquiries, and strengthen collaborative research. Given the scope of this task,  
 87 implementation will necessarily proceed in phases.



88 **Figure 1. Illustration of the lateral groundwater flow, the critical zone of water table depth,**  
 89 **and the coupling strategy between ParFlow and land surface models. Modified from**  
 90 **Yang et al. (2023).**  
 91

92 In this paper, we begin by reviewing key insights gained from two decades of research  
 93 involving ParFlow-based coupled modeling systems. Building on this foundation, we highlight  
 94 how increasing model complexity and functionality are driving a shift toward a next-generation  
 95 coupling paradigm. We then present a re-coupling of the latest versions of ParFlow (PF) and  
 96 CoLM, focusing on core functionalities of CoLM to demonstrate feasibility and highlight  
 97 improvements in overall model performance. This science-oriented integration of basic  
 98 modules—built upon the original coupling interface—serves as a foundation for broader re-  
 99 coupling efforts that will incorporate additional functional components under a redesigned,  
 100 sustainable coupling framework. It also helps us better understand how both models have  
 101 evolved since their original coupling in 2005, thereby informing the development of a next-  
 102 generation framework. In recognition of the increasing number of LSMs being coupled with  
 103 ParFlow, we further propose a ParFlow-Land Surface Coupled Model Intercomparison Project  
 104 (PLCMIP) to promote collaboration and knowledge exchange across the community.

## 105 **2. A brief review of ParFlow-Land/Atmosphere coupled modeling**

106 The coupled model provides a more realistic representation of groundwater dynamics than  
 107 traditional LSMs, while also offering more advanced ecohydrological processes at the land  
 108 surface than conventional groundwater models. Over the past two decades, its major scientific  
 109 contributions can be summarized in three key areas:



- 110 1. It captures the feedbacks from groundwater to land and atmospheric processes—an
- 111 area often overlooked or omitted in both atmospheric and groundwater research
- 112 communities.
- 113 2. It highlights the critical range of water table depth (WTD) that mediates these feedbacks.
- 114 3. It elucidates the impacts of land cover and climate change on groundwater and other
- 115 complex ecohydrological interactions.

## 116 **2.1 Feedbacks from groundwater to land surface and atmosphere**

117 A major consensus in the community is that the representation of groundwater in ESMs  
 118 significantly affects the spatiotemporal distribution of soil moisture, thereby influencing surface  
 119 turbulent fluxes such as latent and sensible heat, as well as the spatiotemporal dynamics of the  
 120 atmospheric boundary layer (Forrester and Maxwell, 2020; Rihani et al., 2015). This is primarily  
 121 due to the limited simulation depth in LSMs and the absence of lateral groundwater flow. The  
 122 former limits drainage in ridge areas, resulting in insufficient water release and an  
 123 overestimation of soil moisture; the latter suppresses groundwater convergence in valley areas,  
 124 leading to underestimation of soil moisture there.

125 Generally, lateral groundwater flow enhances soil moisture in topographic lows,  
 126 suppresses boundary layer development, and increases the evaporative fraction, thereby  
 127 weakening land–atmosphere coupling and reducing near-surface temperatures (Forrester and  
 128 Maxwell, 2020; Keune et al., 2016). These responses are further modulated by the subsurface  
 129 hydraulic conductivities ( $K$ ), with more pronounced sensitivities to  $K$  under simplified  
 130 groundwater parameterizations (Williams and Maxwell, 2011; Keune et al., 2016; Rihani et al.,  
 131 2010). Notably, the impact of groundwater and subsurface properties on surface flux  
 132 partitioning and boundary layer development tends to be most pronounced in the afternoon,  
 133 when radiative forcing peaks and land–atmosphere interactions intensify (Rahman et al., 2015;  
 134 Rihani et al., 2015; Forrester and Maxwell, 2020; Maxwell et al., 2007).

135 Forrester and Maxwell (2020) conducted WRF-based weather simulations over the  
 136 mountainous regions of Colorado to investigate the impact of different lower boundary  
 137 conditions, providing a detailed explanation of the processes mentioned above. The study  
 138 included a baseline scenario and several comparative scenarios, with particular emphasis on  
 139 one that used PF-WRF to explicitly represent three-dimensional groundwater flow. In the  
 140 baseline scenario, conventional WRF simulation was employed, with the subsurface depth of  
 141 2 m, divided into four layers with thicknesses of 0.1, 0.3, 0.6, and 1 m from top to bottom. The  
 142 bottom boundary used the native Noah model setting, which allows free drainage and further  
 143 adjusts fluxes based on terrain. In the PF-WRF scenario, the subsurface depth was increased  
 144 to 102 meters by adding a fifth layer of 100 m in thickness, with the bottom boundary set as  
 145 impermeable. The Noah model and ParFlow were coupled through the top four layers, resulting  
 146 in a coupling depth of 2 m.



Simulation results showed that in the PF-WRF scenario, the enhanced drainage in ridge areas and lateral groundwater convergence led to a decrease in soil moisture over ridges and an increase over valleys. Correspondingly, the boundary layer height also exhibited increases in ridge areas and decreases in valley areas. These changes in soil moisture and boundary layer height showed significant seasonal variations. Furthermore, the results revealed that under the influence of microtopography, the local variation of soil moisture was highly heterogeneous, weakening the general trend of soil moisture varying with elevation as seen in the baseline scenario.

Additionally, in the baseline scenario, the coupling strength between evaporative fraction (EF, the ratio of latent heat to the sum of latent and sensible heat) and boundary layer height was weakened or even reversed in the PF-WRF scenario. That is, the significant negative correlation between EF and boundary layer height decreased or turned positive; this may be due to the temporal variations in EF caused by lateral flow. Moreover, the PF-WRF scenario with lateral flow showed stronger morning mountain breezes (upslope) and valley breezes (downslope), which may have enhanced mountain-valley circulation. Lateral groundwater flow also modulated low-level convection in river valleys, particularly increasing convective available potential energy (CAPE) in the afternoon, thereby perturbing regional precipitation.

Keune et al. (2016) conducted simulations over the European CORDEX region using the TerrSysMP modeling system (Shrestha et al., 2014), setting up two scenarios: one with fully three-dimensional groundwater flow (3D) and the other with one-dimensional free drainage (FD). Similarly, their results revealed that different representations of groundwater led to variations in CAPE, indicating influences on the evolution of atmospheric boundary layer and free troposphere. The 3D scenario weakened land–atmosphere coupling, thereby suppressing the occurrence of extreme weather events, which is consistent with the findings of Forrester and Maxwell (2020). More specifically, the simulated 2 m air temperature was generally lower in the 3D scenario than in the FD scenario, providing useful insights for simulating European heatwaves during the study period.

The study also showed that model differences were primarily located in areas with shallow water tables (depth < 5 m), which aligns with findings of Forrester and Maxwell (2020) that humidity, potential temperature, and vertical wind exhibit more pronounced differences in mountainous valley regions. In addition, the study revealed that variations in deep soil (depth > 3 m) hydraulic conductivities led to discrepancies in simulation results. The FD scenario was more sensitive to the choice of conductivity values, suggesting that simplified physical representations may further amplify the impact of parameter uncertainty.

Williams and Maxwell (2011), using coupled PF-WRF simulations, further explored the feedbacks of geological conditions on land–atmosphere processes such as latent heat flux and wind speed. Based on idealized scenarios, they conducted ensemble simulations by perturbing the hydraulic conductivity field. The results showed that conditioning the hydraulic conductivity significantly reduced uncertainties in simulating land–atmosphere interactions compared to



unconditioned cases. The ensemble mean was closer to the control scenario; for instance, the mean and distribution of simulated wind speed showed reduced uncertainty. These findings provide important implications for various wind energy applications.

## 2.2 The critical zone of WTD in groundwater–land interactions

As discussed above, numerous studies have revealed feedbacks of groundwater on land–atmosphere processes. A key scientific question thus arises: what is the quantitative relationship between land surface states/fluxes and the WTD? Maxwell and Condon (2016), in their study over the continental US, confirmed the critical role of lateral groundwater flow in modulating the partitioning between evaporation (E) and transpiration (T). This influence is most pronounced when the WTD lies between 0.5 and 5 m. Shallower WTD leads to elevated bare-soil evaporation and transpiration, while deeper WTD suppresses both fluxes. Notably, in regions where bare-soil evaporation is limited and transpiration is sustained, the T/E ratio peaks.

Similarly, many studies using PF-CLM have identified a critical WTD range within which land surface variables—such as latent heat flux, sensible heat flux, and surface temperature—are highly sensitive to WTD but exhibit diminished sensitivity beyond this range (Figure 1). For instance, Ferguson’s work over the Little Washita watershed suggests a critical WTD range of approximately 1–10 m (Ferguson and Maxwell, 2012, 2011, 2010), while Yang et al. (2020); Yang et al. (2023) reported comparable results over the North China Plain. Rihani et al. (2015) also illustrate the coupling between WTD and planetary boundary layer depth in this transition zone from ridges to valleys along hillslopes. Generally, when WTD is shallower than this range, soil is nearly saturated and energy availability becomes the limiting factor, weakening the sensitivity of surface states/fluxes to WTD. Conversely, when WTD exceeds this range, gravity-driven drainage dominates, limiting moisture availability and again reducing sensitivity. The upper bound of this range is typically <1 m, while the lower bound often aligns with the model’s coupling depth (Kollet and Maxwell, 2008). However, in some cases, such as Maxwell and Condon (2016), the lower bound extends beyond the nominal 2 m coupling depth, likely due to capillary rise from the water table.

This critical WTD range varies across regions, influenced by differences in subsurface characteristics and rooting depth, though current understanding remains limited. Fan et al. (2017), through analysis of over 2,200 global root depth observations and model-based inversion, showed that rooting depth is regulated by the capillary rise zone. Even within the same species and climate, rooting depth may vary with WTD conditions. In some environments, vegetation develops both shallow fibrous roots and deep taproots to access water under varying conditions—shallow roots for near-surface moisture during wet periods, and deep roots for capillary water during droughts. On well-drained uplands, rooting depth is controlled by infiltration and may not reach significant depths. In contrast, in shallow groundwater zones, oxygen stress may inhibit root growth and decouple vegetation from groundwater. This adaptive rooting strategy suggests that in natural systems, the depth and intensity of groundwater–land surface coupling may exceed what models typically simulate.



Maxwell et al. (2007) further investigated how groundwater feedbacks on land surface processes change under different climate change scenarios, including hot, hot and dry, and hot and wet. It is not difficult to infer that changes in latent heat flux and recharge (precipitation minus ET) within the critical WTD range exhibit strongest spatial variability. Generally, these findings suggest that groundwater feedbacks on land surface processes are closely linked to topographic and climatic conditions. For instance, in the aforementioned mountainous regions of Colorado, spatial variability in WTD leads to diverse groundwater–land surface interactions. The transitional zones between ridges and valleys are often the key areas for such interactions. In humid regions, the water table often follows surface topography (Gleeson et al., 2011), facilitating strong groundwater–land surface coupling. However, in arid regions, WTD may exceed the lower bound of the critical range, reducing the significance of groundwater feedbacks. In natural systems, this interaction is often governed by the complex interplay between climate, topography, geology, and vegetation.

### 2.3 The impacts of land cover and climate changes on groundwater

Climate change has exacerbated mountain pine beetle infestations, leading to widespread tree mortality in the Rocky Mountains (Bearup et al., 2014). Mikkelsen et al. (2013) studied the impacts of beetle-induced forest dieback on water and energy balances at the hillslope scale using PF-CLM simulations. An idealized hillslope model (500 m × 1000 m × 12.5 m) was used, with scenarios representing different stages of infestation—green, red, grey, and dieback—by modifying the leaf area index and stomatal conductance. Simulation results showed similar levels of ET across all scenarios in winter, but significantly higher ET in summer under the green scenario, primarily due to transpiration. In contrast, the other scenarios exhibited lower ET limited by soil moisture availability, with evaporation being the dominant process. The dieback scenario produced the highest peak in snow water equivalent (SWE), and reduced canopy cover allowed more solar radiation to penetrate, accelerating snowmelt. This earlier and more rapid melt resulted in earlier and higher streamflow peaks, as well as increased subsurface storage. A related particle tracking study (Bearup et al., 2016) further demonstrated greater groundwater contributions to streamflow during late summer.

Condon et al. (2020) conducted a continental-scale simulation across the United States using the PF-CLM CONUS 1.0 model (Maxwell et al., 2015) to examine groundwater responses to 1°C, 2°C, and 4°C warming scenarios. Warming was found to enhance ET, with shallow groundwater providing supplementary moisture to meet the increased demand, thereby partially mitigating land surface water stress. However, prolonged warming ultimately led to continuous groundwater depletion and a decoupling of groundwater from land surface processes. The magnitude of ET increases, and groundwater storage loss varied with WTD, with the strongest responses occurring within the previously identified critical WTD range. Overall, the humid eastern U.S. exhibited greater sensitivity to warming than the arid western regions. These findings highlight the risk of underestimating groundwater–land surface feedbacks when using simplified groundwater parameterizations in ESMs.





## 264 **2.4 Enhanced LSM functionality motivates recoupling**

265 These selected representative studies have demonstrated the critical role of groundwater  
 266 in Earth system processes. Over the past two decades, CoLM—like many other LSMs—has  
 267 undergone substantial development, including functional extensions, improved  
 268 parameterization schemes, and the introduction of multiple alternative process representations.  
 269 However, our understanding of how groundwater interacts with these additional processes—  
 270 including how various parameterizations respond to and influence groundwater dynamics—  
 271 remains limited. These limitations underscore the pressing need to upgrade the coupling  
 272 between ParFlow and LSMs. The key scientific advances of CoLM are summarized as follows  
 273 (Yuan and Dai, 2025):

274 **(1) Radiation transfer:** a three-dimensional vegetation shortwave (Yuan et al., 2014) and  
 275 longwave radiation transfer scheme has been incorporated, the SNICAR snow radiation  
 276 transfer scheme has been added to simulate snow albedo and radiation absorption within the  
 277 snowpack, and an improved two-stream approximation scheme for vegetation radiation transfer  
 278 has been provided (Yuan et al., 2017). **(2) Turbulent fluxes:** the model enhances the continuity  
 279 of dynamic parameters and processes across transitions from dense to sparse vegetation.  
 280 Resistance coefficients below the canopy are calculated using a profile integration method. A  
 281 new turbulent exchange scheme supports multiple coexisting plant functional types (PFTs)  
 282 within a three-dimensional canopy. Several soil resistance parameterizations are provided to  
 283 improve surface evapotranspiration estimates. Additionally, a surface turbulent flux scheme has  
 284 been introduced to account for large-eddy effects. **(3) Canopy interception and plant**  
 285 **hydraulics:** the model includes multiple canopy interception schemes and a plant hydraulics  
 286 module governed by Darcy's law. Different parameterizations emphasize distinct physical  
 287 processes and support investigation of the evolution, drivers, and trends of interception under  
 288 varying conditions. The hydraulics module replaces empirical formulations that relate plant  
 289 stress to soil water potential and improves the simulation of land-atmosphere water exchange  
 290 under changing environments. **(4) Leaf temperature:** A simplified one-dimensional two-big-  
 291 leaf scheme has been implemented to improve the numerical stability of leaf temperature  
 292 simulations. In addition, a new parameterization has been developed for leaf temperature in  
 293 multi-PFT scenarios with a three-dimensional canopy structure. **(5) Other functional**  
 294 **extensions:** additional modules have been developed for biogeochemistry, urban systems,  
 295 crop modeling, land use and land cover change, wildfire, ozone-related ecophysiological stress,  
 296 and integrated hydrological processes.

## 297 **3. Foundational step toward sustainable coupling**

298 To explore the feasibility of re-coupling the latest versions of ParFlow and CoLM, we  
 299 conducted a preliminary integration of the two models. This effort focuses exclusively on the  
 300 basic water and energy modules of CoLM and is built upon the existing ParFlow-CLM coupling  
 301 interface. Our goal is to understand how both models have advanced over the past two decades,  
 302 in terms of functionality, code architecture (e.g., parallelism), data structures, I/O interfaces,





303 and pre-/post-processing tools. This process also helps identify key variables and processes—  
 304 along with their implementation in code—that are critical for a more comprehensive coupling  
 305 effort. Although this re-coupling effort uses CoLM as an example, the experience and insights  
 306 gained are also applicable to coupling ParFlow with other LSMs.

307 This initial re-coupling serves to evaluate model performance with respect to physical  
 308 processes, particularly highlighting potential improvements gained through two decades of  
 309 development. It also establishes a set of benchmarks for testing and debugging as more CoLM  
 310 modules are progressively incorporated. Without this incremental approach, the complexity of  
 311 multiple physical processes would make testing and debugging considerably challenging. In  
 312 addition, we fully leverage the lessons learned through trial and error over the past twenty years  
 313 to ensure a more stable execution of the coupled model (Ferguson et al., 2016). While this  
 314 phase emphasizes gaining a deeper understanding of the physical processes, future work on  
 315 sustainable coupling will likely shift toward technical aspects—such as refining the coupling  
 316 interface, improving modularity, and ensuring long-term maintainability. These efforts will  
 317 collectively inform our understanding of the challenges and opportunities involved in  
 318 establishing a sustainable coupling framework.

### 319 **3.1 Model setup, experimental design, and evaluation data**

320 The modeling domain, selected from the CONCN domain (Yang et al., 2025), is located in  
 321 the North Pearl River Basin (Figure 2). This area was chosen as it serves as a demonstration  
 322 area for the CONCN model and possesses more complete infrastructure e.g., the processed  
 323 ERA5-Land reanalysis data (Muñoz-Sabater et al., 2021). Since the CONCN model and CoLM  
 324 use four and ten soil layers, respectively, the CONCN model structure was adjusted to align  
 325 with CoLM's vertical discretization. The ParFlow model employed in this study comprises 11  
 326 layers: the top 10 layers match CoLM in thickness, while the additional 11th layer represents  
 327 the deep aquifer. ParFlow and CoLM are coupled through the top 10 layers. The coupled model  
 328 maintains a horizontal resolution of ~1 km, consistent with the CONCN model and includes 252  
 329 and 146 grid cells in the *x* and *y* directions, respectively. This corresponds to a spatial extent of  
 330 approximately 242.35 km (*x direction*) × 140.41 km (*y direction*) × 103.43 m (*z direction*). Soil  
 331 properties for CoLM inputs were derived from the Global Soil Dataset for Earth System  
 332 Modeling (GSDE) (Shangguan et al., 2014). Soil parameters for ParFlow were reconstructed  
 333 based on the sand and clay weight percentages from the same GSDE dataset, following the  
 334 USDA soil classification system. Properties for the 11th layer were obtained from GLHYMPS  
 335 1.0 (Gleeson et al., 2011; Gleeson et al., 2014), as used in the CONCN model. The *e*-folding  
 336 of aquifer hydraulic conductivity with depth was implemented using a characteristic depth of 50  
 337 m (Fan et al., 2007). Other surface input parameters—including Manning's roughness  
 338 coefficients, topographic slopes, and land cover types—were adopted directly from the CONCN  
 339 model configuration (Yang et al., 2025).

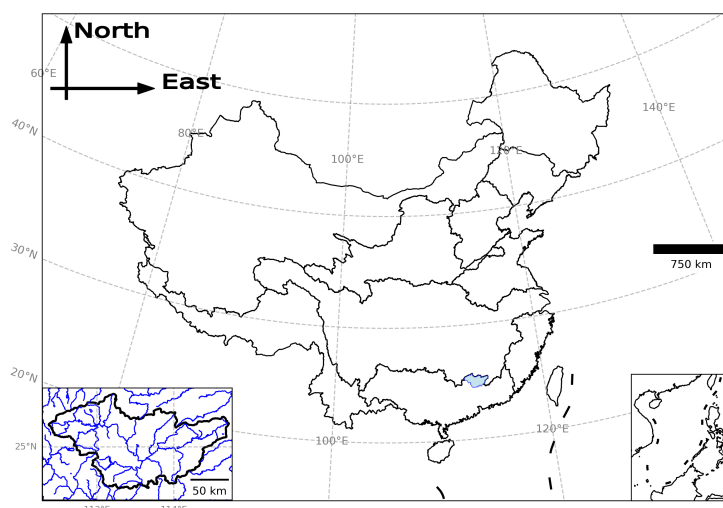


**Figure 2. Location of the modeling domain**

340  
 341

342 We first spun up the standalone ParFlow model using potential recharge data clipped from  
 343 the CONCN domain. Then we drove the coupled model using the 2018 meteorological forcing  
 344 from ERA5-Land reanalysis. However, this is an area with limited snow. To demonstrate snow  
 345 performance, we created a synthetic case by applying the water year 2003 forcing from a  
 346 station (Defnet et al., 2024) located in Colorado to a single column model. To evaluate changes  
 347 in model performance, we also constructed 11-layer models (with 10 coupled layers) using the  
 348 old ParFlow-CLM for both real-world and synthetic cases. We compared the simulated sensible  
 349 heat, latent heat, skin temperature, transpiration, SWE, and the water flux exchange between  
 350 the new and old models (Figures 3 and 4). Here, water flux exchange refers to the source/sink  
 351 terms in Richards' equation: positive values represent infiltration, while negative values are  
 352 caused by ET. We also evaluated the simulation performance of the first four variables using  
 353 ERA5-Land reanalysis. For the synthetic cases, we used data from the Snow Telemetry  
 354 (SNOTEL) network maintained by the Natural Resources Conservation Service (NRCS)—  
 355 specifically, the measured SWE at the same location as the meteorological forcing—to evaluate  
 356 the models' overall ability to simulate the timing and magnitude of snowpack.

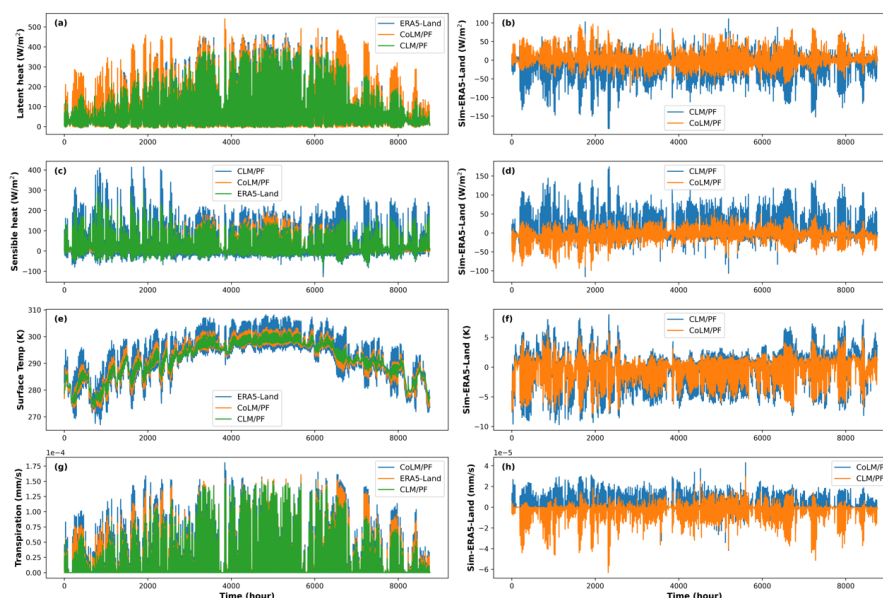


**Figure 3.** Comparison of latent heat flux, sensible heat flux, surface temperature, and transpiration between the old CLM/ParFlow and the new CoLM/ParFlow models. The corresponding values from ERA5-Land are plotted in the left column for reference. The right column shows the differences between the model simulations and ERA5-Land for each variable. Each subplot represents spatial averages over the entire modeling domain. For clarity and to prevent overlapping, the plotting order is intentionally varied across subplots.

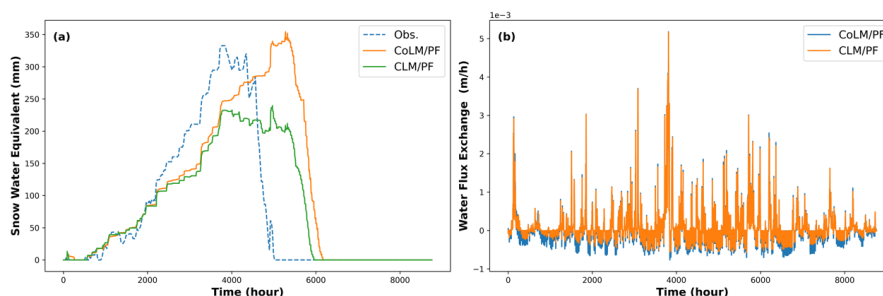


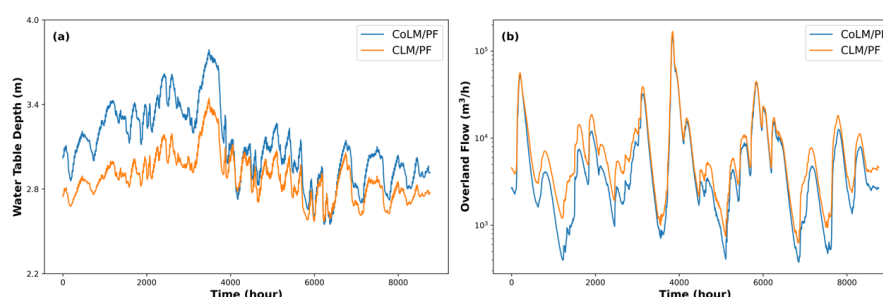
**Figure 4.** (a) shows the simulated snow water equivalent from the CoLM/ParFlow and CLM/ParFlow single column models, compared against SNOTEL observations. (b) presents the spatially averaged net water fluxes from CoLM and CLM to ParFlow, representing the source and sink terms in the ParFlow domain; both fluxes represent spatial averages over the entire modeling domain.

### 3.2 Performance gains from updated CoLM support recoupling

Simulations of all variables by CoLM/PF exhibit improved performance relative to CLM/PF when evaluated against ERA5-Land reanalysis data (Figure 3). CoLM/PF produces a more realistic partitioning of turbulent fluxes, characterized by increased latent heat and reduced sensible heat (Figures 3a and 3c). Notably, transpiration simulated by CoLM/PF is substantially higher and aligns more closely with ERA5-Land data (Figure 3g). Additionally, CoLM/PF more



378 accurately reproduces the fluctuations in land surface temperature compared to CLM/PF  
 379 (Figure 3e). In the single column simulations (Figure 4a), CoLM/PF also generates a higher  
 380 peak SWE than CLM/PF, showing better agreement with SNOTEL observations, although both  
 381 models display deviations in the timing of SWE accumulation. This discrepancy may stem from  
 382 the idealized subsurface configurations used in both models. Improvements in both  
 383 transpiration and SWE are further supported by previous research; for instance, O'Neill et al.  
 384 (2021) reported consistently lower ET and SWE from CLM/PF in the assessment of CONUS  
 385 1.0 model. The overall advancement in model performance can likely be attributed to the more  
 386 sophisticated process representations embedded in CoLM.



387  
 388 **Figure 5. (a) and (b) show the simulated water table depth and overland flow by**  
 389 **CoLM/ParFlow and CLM/ParFlow, respectively. Each subplot represents spatial**  
 390 **averages over the entire modeling domain.**

391 Figure 4b illustrates the net fluxes transferred from the land surface to the subsurface,  
 392 which directly influence hydrologic dynamics such as WTD and overland flow. These exchange  
 393 fluxes show greater variability in the CoLM/PF simulation, suggesting more dynamic surface–  
 394 subsurface interactions. Consistent with this, Figure 5 reveals more pronounced temporal  
 395 variability in both WTD and overland flow. A generally deeper water table is observed in  
 396 CoLM/PF (Figure 5a), which is likely a result of the higher plant water uptake, i.e., increased  
 397 transpiration, depicted in Figures 3a, 3g and 4b. Consequently, the reduction in baseflow from  
 398 groundwater may explain the observed decrease in low levels of overland flow (Figure 5b).

399 To improve the representation of turbulent exchanges between the vegetation canopy and  
 400 the atmosphere, the model employs a profile-integrated approach to resolve key dynamical  
 401 parameters (e.g., turbulent diffusivity  $K(z)$ ) with explicit vertical resolution. In particular,  
 402 resistance-related variables—such as displacement height ( $d$ ) and roughness length ( $z_0$ ), which  
 403 characterize canopy-atmosphere momentum exchange, as well as aerodynamic resistances  
 404 for leaves ( $r_b$ ) and ground surface ( $r_d$ ), which govern within-canopy and near-surface heat and  
 405 vapor transfer—are refined to account for structural heterogeneity. Meanwhile, profile-  
 406 integrated functions are dynamically computed based on vegetation structure and atmospheric  
 407 stability, and directly determine resistance terms (e.g.,  $r_{ah}$ ,  $r_{aw}$ ). This also includes revised  
 408 roughness length formulations that explicitly account for atmospheric stability, extending  
 409 beyond the original neutral-based assumptions in schemes such as Raupach (1994, 1992).  
 410 This combined approach yields a more physically consistent and vertically continuous



411 treatment of turbulent fluxes under non-neutral stratification, enhancing realism in complex  
 412 canopy conditions. In addition, other schemes—such as those related to soil thermal  
 413 parameters (including heat capacity and heat conductivity), as well as soil color and associated  
 414 reflectance—also differ between the CoLM/PF and CLM/PF models. All of these differences  
 415 motivate a coupled model intercomparison project to evaluate how different schemes, either  
 416 within a single model or across different models, affect the performance of the coupled model  
 417 and land–hydrology process interactions.

418 In this initial coupling process, we found that the main changes were related to data  
 419 structure, module organization, module names, and variable naming conventions. For example,  
 420 structures were broken down into multiple arrays, modules were split and reorganized based  
 421 on functionality, some modules were removed from the main program and used as  
 422 preprocessing components, and module adjustments were often accompanied by renaming. A  
 423 large number of variable names were also changed. Moreover, the inclusion of multiple  
 424 parameterization schemes has increased code complexity to some extent, resulting in  
 425 significantly larger module sizes. Nevertheless, most physical processes have retained their  
 426 original core parameterizations. This means that the primary task in this initial coupling stage  
 427 is to identify the key physical processes and the critical variables within the new system  
 428 structure. Several new parameterization schemes have also been implemented—for example,  
 429 those associated with the turbulent exchange discussed above—though the application of other  
 430 schemes will require further testing in future work.

#### 431 **4. A sustainable recoupling framework for future development**

432 Here, we propose a sustainable framework for future CoLM/ParFlow coupling based on  
 433 our preliminary work (Figure 6). This framework consists of four key components: a coupler-  
 434 based architecture, a robust initial foundation, protocols for scalable upgrades, and a  
 435 community interaction platform.

##### 436 **• Coupler-based architecture for long-term sustainability**

437 While the current ParFlow-Land interface built in ParFlow supports efficient coupling with  
 438 land surface and atmospheric models, demonstrates good parallel performance, and avoids  
 439 the overhead associated with inter-model communication, it lacks compatibility with  
 440 standardized coupling frameworks and protocols. This limits the integration of coupled models  
 441 into broader Earth system modeling frameworks. In contrast, coupler-based architectures—  
 442 such as ESMF/NUOPC, CESM/cpl7, and OASIS3-MCT—are now standard in modern Earth  
 443 system modeling. They preserve the native data structures, domain decomposition, and parallel  
 444 logic of each model, which is particularly important given the substantial structural differences  
 445 between ParFlow and CoLM. For instance, this approach allows retaining ParFlow's GPU-  
 446 based parallelism (Hokkanen et al., 2021) and CoLM's MPI-based structure, along with their  
 447 respective domain decomposition strategies. It also enables continued use of each model's  
 448 preferred data format and processing tools—for example, ParFlow's `.pfb` format and `pftools`,



as well as CoLM's NetCDF-based workflow. Adopting a standardized coupler thus facilitates modular development, cross-system compatibility, and long-term maintainability. Looking forward, such coupler-based designs could also be extended to support surrogate model integration (Bennett et al., 2024; Tran et al., 2021), enabling hybrid workflows that combine physical models and AI-based components.

#### • **Strong foundations through early-stage mapping**

Laying a solid foundation during the initial coupling phase is critical. First, a mapping between ParFlow's grid and CoLM's subgrids must be established to support future model extensions. The current coupling only supports integration based on the LCT (Land Cover Type) subgrid, whereas important functional extensions such as biogeochemistry and 3D vegetation canopy processes rely on plant function types (PFTs) and the associated PFT and PC (Plant Community) subgrids. The mapping between grids of different models is a key concern in the coupling community and directly affects coupling performance (Valcke, 2022). Currently, most approaches rely on physical interpolation methods; incorporating an AI-based scale transformation layer with mass conservation constraints could be a promising enhancement. Second, key variables and processes from newly introduced modules or previously untested parameterizations must be identified. For example, the plant hydraulics module requires soil hydraulic conductivity fields, which are not included in the current coupling interface. More importantly, a structured logging system should be implemented to track all exchanged variables, their associated modules, and the corresponding grid structures, thereby ensuring transparency and traceability throughout development.

#### • **Protocols for efficient and maintainable coupler upgrades**

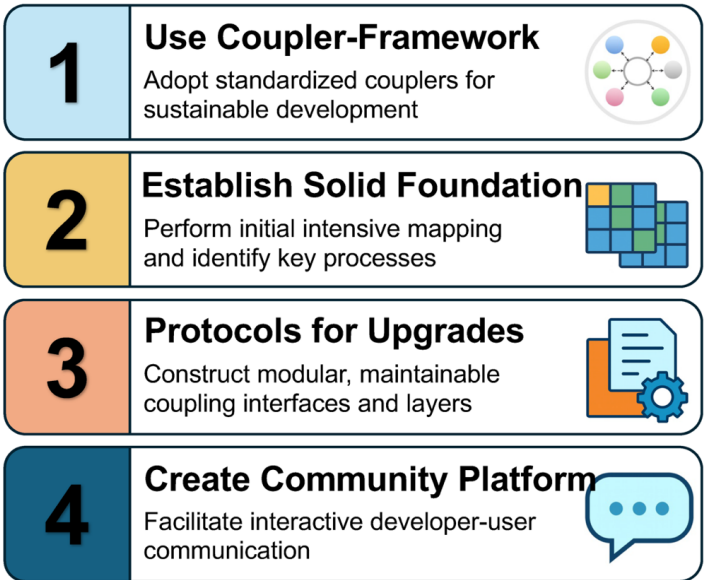
Two key aspects are emphasized. First, the architecture of interfaces and coupling layers should be designed for long-term clarity and ease of maintenance. Taking ESMF/NUOPC as an example, the model-side interfaces and coupler-side connector and mediator layers are implemented with a focus on modular organization, encapsulated data exchange, and well-structured control flow, ensuring that the system can be reliably extended as new model features or physical processes are introduced. Second, developers introducing new modules, parallelization strategies, or grid structures, within one model must explicitly assess their potential impact on the other model, clarify any newly introduced variables or data structures to be exchanged via the coupler, and submit pull requests with corresponding explanations. Senior maintainers should review these changes and provide targeted feedback on necessary updates to the interface and coupling logic. All modifications affecting model interaction must be tracked in the logging system described above, and no update should be considered complete until it is formally registered in the log.

#### • **Community platform for collaboration and maintenance**

A dedicated community platform—such as a GitHub repository, mailing list, or model portal—should be established to support developer–user interaction, technical discussion, and



487 feedback collection. This platform will also serve to announce new model releases, coupling  
488 layer updates, or changes in the logging system. Transparent communication and community-  
489 driven collaboration are essential for the long-term sustainability and extensibility of the coupled  
490 model system. Looking forward, we envision extending this platform into a broader, community-  
491 driven environment for managing and operating ParFlow–LSM coupled models, drawing  
492 inspiration from efforts such as eWaterCycle (Hut et al., 2022). Beyond supporting collaboration  
493 and information sharing, such a platform could streamline model configuration, coupling  
494 workflows, data exchange, and reproducibility—thereby accelerating adoption, improving  
495 transparency, and fostering integration across hydrological and Earth system science  
496 communities. This would also address a current gap, as ParFlow-based coupled systems  
497 remain largely fragmented and lack standardized tools for integration, testing, and  
498 dissemination.



499  
500 **Figure 6. The coupling framework for sustainable development**

501 **5. ParFlow-Land coupled model intercomparison project (PLCMIP)**

502 Over the past decades, numerous land and/or atmosphere models coupled with ParFlow  
503 have been developed (Table 1). These models vary in their functional capabilities and adopt  
504 different coupling strategies, which may significantly affect computational efficiency. The two  
505 models coupled with CoLM aim to understand the fundamental interactions of water and energy  
506 between subsurface and land surface processes (Dai et al., 2003; Maxwell and Miller, 2005).  
507 In contrast, the two models coupled with ARPS and WRF (Maxwell et al., 2007; Maxwell et al.,  
508 2011; Skamarock and Klemp, 2008; Xue et al., 2000; Xue et al., 2001), along with the two  
509 generations of TerrSysMP (Shrestha et al., 2014; Oleson et al., 2008; Lawrence et al., 2019;  
510 Poll et al., 2024), provide capabilities to explore two-way feedbacks across each interface within





the subsurface–land surface–atmosphere system. Furthermore, the coupling of ParFlow with TREES (Tai et al., 2018; Mackay et al., 2015) and ELM-FATES (Fang et al., 2022; Caldwell et al., 2019; Fisher et al., 2015; Leung et al., 2020) introduces advanced vegetation dynamics into land surface process representations. Finally, integration with NASA-LIS enables data assimilation within the coupled modeling framework (Maina et al., 2025; Kumar et al., 2008; Niu et al., 2011), and TerrSysMP also incorporates the PDAF (Parallel Data Assimilation Framework) to support data assimilation capabilities (Kurtz et al., 2016).

Model intercomparison provides a valuable means to assess model development and foster connections or collaborations across research communities. Several well-known intercomparison projects exist, such as the Coupled Model Intercomparison Project (CMIP) for ESM intercomparison (Eyring et al., 2016), and the Land Surface, Snow and Soil Moisture Model Intercomparison Project (LS3MIP) (Van Den Hurk et al., 2016), which is designed to assess the performance of land modules in current ESMs. In addition, individual intercomparison activities have also been widely conducted within the land surface modeling community (Scanlon et al., 2018; Liu et al., 2023). ParFlow has also participated in various model intercomparison projects involving hydrologic models and individual studies, such as those by Maxwell et al. (2014); Sulis et al. (2017); Kollet et al. (2017); Sulis et al. (2010). Given the differences among the ParFlow-based coupled models mentioned above, a dedicated model intercomparison project (MIP) is needed to systematically evaluate coupled models and support the development of a community platform for benchmarking and collaboration, with the following objectives:

(1) To quantify the strength and spatiotemporal variability of groundwater–land–atmosphere interactions resulting from different parameterization schemes used in various land surface and atmospheric models.

(2) To compare computational efficiency across different coupling strategies.

(3) To identify the unique functionalities and strengths of each coupled model, providing users with guidance in selecting the most appropriate model for their specific research needs.

## 6. Summary

Twenty years after the original ParFlow-CLM coupling (Maxwell and Miller, 2005), this study reaffirms the long-term scientific and technical significance of that foundational effort. Over two decades, the coupled system has made major contributions in establishing the critical role of groundwater in modulating subsurface–land–atmosphere feedbacks and identifying the existence of a critical water table depth range that governs these bidirectional interactions. Technically, this coupling demonstrated a viable approach for integrating a groundwater model with a land surface scheme—the lower boundary of Earth system models—thereby providing a template for incorporating groundwater processes into ESMs. To revisit and update this legacy, we carried out a preliminary re-coupling of the latest versions of ParFlow and CoLM,



548 focusing on core water and energy processes. This re-coupling already reveals improved model  
549 performance and provides a functional platform for incremental expansion and benchmarking.

550 Looking forward, developing a sustainable ParFlow–LSM coupling framework will require  
551 a more comprehensive and community-oriented design. This includes adopting a lightweight  
552 coupler architecture that preserves each model's native data structures, parallel strategies, and  
553 processing tools, while supporting modular integration of new physical or surrogate  
554 components. To support long-term maintainability and usability, we envision a shared platform  
555 that integrates model configuration, coupling workflows, data exchange, and benchmarking  
556 functions. Such a platform would enhance transparency, reproducibility, and ease of adoption  
557 across the hydrologic and Earth system modeling communities. In parallel, we propose  
558 launching a model intercomparison project (PLCMIP) to systematically evaluate performance,  
559 compare coupling strategies, and guide future development.

560

561



562

**Table 1. ParFlow and Land/Atmosphere coupled models**

<b>Coupled model</b>	<b>Model description</b>	<b>Coupling approach</b>	<b>Reference</b>
CoLM	The Common Land Model	CoLM as a subroutine	<b>Maxwell and Miller, 2005;</b> Dai et al., 2003
ARPS	The mesoscale atmospheric model Advanced Regional Prediction System; coupled with the built-in land surface model	ARPS as a subroutine	<b>Maxwell et al., 2007;</b> Xue et al., 2000, 2001
WRF	The community numerical weather prediction Weather Research and Forecasting model, version 3.0; coupled with the built-in Noah model	WRF as a subroutine	<b>Maxwell et al., 2011;</b> Skamarock and Klemp, 2008
CLM3.5	The NCAR Community Land Model (version 3.5) in TerrSysMP	<b>Coupler.</b> Ocean Atmosphere Sea Ice Soil, version 3.0 (OASIS3)	<b>Shrestha et al., 2014;</b> Oleson et al., 2008
TREES	A plant physiology model: Terrestrial Regional Ecosystem Exchange Simulator	TREES as a subroutine	<b>Tai et al., 2018;</b> Mackay et al., 2015
ELM	The Energy Exascale Earth System Model (E3SM) land model (ELM) that includes the Functionally Assembled Terrestrial Ecosystem Simulator (FATES)	ParFlow as a subroutine	<b>Fang et al., 2022;</b> Caldwell et al., 2019; Leung et al., 2020; Fisher et al., 2015
eCLM	An adaption of the NCAR Community Land Model (version 5.0) in TerrSysMP2	<b>Coupler.</b> OASIS3-MCT, where MCT represents Model Coupling Toolkit	<b>Poll et al., 2024;</b> Lawrence et al., 2019
Noah-MP	Noah-MP in the NASA Land Information System (LIS)	<b>Coupler.</b> The Earth System Modeling Framework and the National United Operational Prediction Capability (ESMF/NUOPC)	<b>Maina et al., 2025;</b> Kumar et al., 2008; Niu et al., 2011
CoLM2024	The Common Land Model, version 2024	CoLM2024 as a subroutine	<b>This study</b>

563



## 564 **Code and data availability**

565 The datasets used in this study are all from public sources and are cited in the main text.  
 566 ParFlow version 3.13, as used in this study, is available at  
 567 <https://doi.org/10.5281/zenodo.4816884> (Smith et al., 2024). The new ParFlow–CoLM model  
 568 and the test cases, including input and output files, are available at  
 569 <https://doi.org/10.5281/zenodo.16879407> (Yang, 2025), and a copy is also available on GitHub  
 570 at <https://github.com/aureliayang/parflow-colm>.

## 571 **Author contributions**

572 Conceptualization: CY and RM. Methodology: CY, YD, and RM. Investigation: CY, AS, SZ,  
 573 YD, SK, and RM. Resources: CY, YD, and RM. Writing (original draft): CY. Writing (review and  
 574 editing): CY, YD, SK, and RM.

## 575 **Competing interests**

576 The contact author has declared that none of the authors has any competing interests.

## 577 **Acknowledgements**

578 We gratefully acknowledge that the work reported in this paper was largely performed using  
 579 the Princeton Research Computing resources at Princeton University, made up of a consortium  
 580 of groups led by the Princeton Institute for Computational Science and Engineering (PICSciE)  
 581 and the Office of Information Technology's Research Computing.

## 583 **References**

- 584 Ashby, S. F. and Falgout, R. D.: A parallel multigrid preconditioned conjugate gradient algorithm  
 585 for groundwater flow simulations, *Nucl Sci Eng*, 124, 145-159, 1996.
- 586 Bearup, L. A., Maxwell, R. M., and McCray, J. E.: Hillslope response to insect-induced land-  
 587 cover change: an integrated model of end-member mixing, *Ecohydrology*, 9, 195-203, 2016.
- 588 Bearup, L. A., Maxwell, R. M., Clow, D. W., and McCray, J. E.: Hydrological effects of forest  
 589 transpiration loss in bark beetle-impacted watersheds, *Nat Clim Change*, 4, 481,  
 590 10.1038/nclimate2198 [https://www.nature.com/articles/nclimate2198#supplementary-](https://www.nature.com/articles/nclimate2198#supplementary-information)  
 591 [information](https://www.nature.com/articles/nclimate2198#supplementary-information), 2014.
- 592 Bennett, A., Tran, H., De la Fuente, L., Triplett, A., Ma, Y., Melchior, P., Maxwell, R. M., and  
 593 Condon, L. E.: Spatio-Temporal Machine Learning for Regional to Continental Scale  
 594 Terrestrial Hydrology, *J Adv Model Earth Sy*, 16, e2023MS004095,  
 595 <https://doi.org/10.1029/2023MS004095>, 2024.
- 596 Caldwell, P. M., Mametjanov, A., Tang, Q., Van Roekel, L. P., Golaz, J.-C., Lin, W., Bader, D.  
 597 C., Keen, N. D., Feng, Y., Jacob, R., Maltrud, M. E., Roberts, A. F., Taylor, M. A., Veneziani,  
 598 M., Wang, H., Wolfe, J. D., Balaguru, K., Cameron-Smith, P., Dong, L., Klein, S. A., Leung,  
 599 L. R., Li, H.-Y., Li, Q., Liu, X., Neale, R. B., Pinheiro, M., Qian, Y., Ullrich, P. A., Xie, S.,  
 600 Yang, Y., Zhang, Y., Zhang, K., and Zhou, T.: The DOE E3SM Coupled Model Version 1:  
 601 Description and Results at High Resolution, *J Adv Model Earth Sy*, 11, 4095-4146,  
 602 <https://doi.org/10.1029/2019MS001870>, 2019.
- 603 Condon, L. E., Atchley, A. L., and Maxwell, R. M.: Evapotranspiration depletes groundwater  
 604 under warming over the contiguous United States, *Nat Commun*, 11, 873, 10.1038/s41467-  
 605 020-14688-0, 2020.
- 606 Dai, Y. J., Zeng, X. B., Dickinson, R. E., Baker, I., Bonan, G. B., Bosilovich, M. G., Denning, A.  
 607 S., Dirmeyer, P. A., Houser, P. R., Niu, G. Y., Oleson, K. W., Schlosser, C. A., and Yang,  
 608 Z. L.: The Common Land Model, *B Am Meteorol Soc*, 84, 1013-1023, 10.1175/Bams-84-8-  
 609 1013, 2003.



- 610 de Graaf, I. E. M. and Stahl, K.: A model comparison assessing the importance of lateral  
611 groundwater flows at the global scale, *Environ Res Lett*, 17, 2022.
- 612 de Graaf, I. E. M., van Beek, R. L. P. H., Gleeson, T., Moosdorf, N., Schmitz, O., Sutanudjaja,  
613 E. H., and Bierkens, M. F. P.: A global-scale two-layer transient groundwater model:  
614 Development and application to groundwater depletion, *Adv Water Resour*, 102, 53-67,  
615 <https://doi.org/10.1016/j.advwatres.2017.01.011>, 2017.
- 616 Defnet, A., Hasling, W., Condon, L., Johnson, A., Artavanis, G., Triplett, A., Lytle, W., and  
617 Maxwell, R.: hf\_hydrodata: A Python package for accessing hydrologic simulations and  
618 observations across the United States, *Journal of Open Source Software*, 9, 6623, 2024.
- 619 Eyring, V., Bony, S., Meehl, G. A., Senior, C. A., Stevens, B., Stouffer, R. J., and Taylor, K. E.:  
620 Overview of the Coupled Model Intercomparison Project Phase 6 (CMIP6) experimental  
621 design and organization, *Geosci. Model Dev.*, 9, 1937-1958, 10.5194/gmd-9-1937-2016,  
622 2016.
- 623 Fan, Y., Miguez-Macho, G., Jobbágy, E. G., Jackson, R. B., and Otero-Casal, C.: Hydrologic  
624 regulation of plant rooting depth, *Proceedings of the National Academy of Sciences*, 114,  
625 10572-10577, 10.1073/pnas.1712381114, 2017.
- 626 Fan, Y., Miguez-Macho, G., Weaver, C. P., Walko, R., and Robock, A.: Incorporating water  
627 table dynamics in climate modeling: 1. Water table observations and equilibrium water table  
628 simulations, *Journal of Geophysical Research: Atmospheres*, 112,  
629 <https://doi.org/10.1029/2006JD008111>, 2007.
- 630 Fan, Y., Clark, M., Lawrence, D. M., Swenson, S., Band, L. E., Brantley, S. L., Brooks, P. D.,  
631 Dietrich, W. E., Flores, A., Grant, G., Kirchner, J. W., Mackay, D. S., McDonnell, J. J., Milly,  
632 P. C. D., Sullivan, P. L., Tague, C., Ajami, H., Chaney, N., Hartmann, A., Hazenberg, P.,  
633 McNamara, J., Pelletier, J., Perket, J., Rouholahnejad-Freund, E., Wagener, T., Zeng, X.,  
634 Beighley, E., Buzan, J., Huang, M., Livneh, B., Mohanty, B. P., Nijssen, B., Safeeq, M.,  
635 Shen, C., van Verseveld, W., Volk, J., and Yamazaki, D.: Hillslope Hydrology in Global  
636 Change Research and Earth System Modeling, *Water Resour Res*, 55, 1737-1772,  
637 10.1029/2018wr023903, 2019.
- 638 Fang, Y., Leung, L. R., Koven, C. D., Bisht, G., Detto, M., Cheng, Y., McDowell, N., Muller-  
639 Landau, H., Wright, S. J., and Chambers, J. Q.: Modeling the topographic influence on  
640 aboveground biomass using a coupled model of hillslope hydrology and ecosystem  
641 dynamics, *Geosci. Model Dev.*, 15, 7879-7901, 10.5194/gmd-15-7879-2022, 2022.
- 642 Ferguson, I. M. and Maxwell, R. M.: Role of groundwater in watershed response and land  
643 surface feedbacks under climate change, *Water Resour Res*, 46, 2010.
- 644 Ferguson, I. M. and Maxwell, R. M.: Hydrologic and land-energy feedbacks of agricultural water  
645 management practices, *Environ Res Lett*, 6, Artn 01400610.1088/1748-9326/6/1/014006,  
646 2011.
- 647 Ferguson, I. M. and Maxwell, R. M.: Human impacts on terrestrial hydrology: climate change  
648 versus pumping and irrigation, *Environ Res Lett*, 7, Artn 04402210.1088/1748-  
649 9326/7/4/044022, 2012.
- 650 Ferguson, I. M., Jefferson, J. L., Maxwell, R. M., and Kollet, S. J.: Effects of root water uptake  
651 formulation on simulated water and energy budgets at local and basin scales, *Environ Earth*  
652 *Sci*, 75, ARTN 31610.1007/s12665-015-5041-z, 2016.
- 653 Fisher, R. A., Muszala, S., Versteinst, M., Lawrence, P., Xu, C., McDowell, N. G., Knox, R.  
654 G., Koven, C., Holm, J., Rogers, B. M., Spessa, A., Lawrence, D., and Bonan, G.: Taking  
655 off the training wheels: the properties of a dynamic vegetation model without climate  
656 envelopes, *CLM4.5(ED)*, *Geosci. Model Dev.*, 8, 3593-3619, 10.5194/gmd-8-3593-2015,  
657 2015.
- 658 Forrester, M. M. and Maxwell, R. M.: Impact of Lateral Groundwater Flow and Subsurface  
659 Lower Boundary Conditions on Atmospheric Boundary Layer Development over Complex  
660 Terrain, *J Hydrometeorol*, 21, 1133-1160, <https://doi.org/10.1175/JHM-D-19-0029.1>, 2020.
- 661 Gleeson, T., Marklund, L., Smith, L., and Manning, A. H.: Classifying the water table at regional  
662 to continental scales, *Geophys Res Lett*, 38, Artn L0540110.1029/2010gl046427, 2011.
- 663 Gleeson, T., Moosdorf, N., Hartmann, J., and van Beek, L. P. H.: A glimpse beneath earth's  
664 surface: GLOBal HYdrogeology MaPS (GLHYMPS) of permeability and porosity, *Geophys*  
665 *Res Lett*, 41, 3891-3898, 10.1002/2014gl059856, 2014.
- 666 Hokkanen, J., Kollet, S., Kraus, J., Herten, A., Hrywniak, M., and Pleiter, D.: Leveraging HPC  
667 accelerator architectures with modern techniques — hydrologic modeling on GPUs with  
668 ParFlow, *Computat Geosci*, 25, 1579-1590, 10.1007/s10596-021-10051-4, 2021.



- Hut, R., Drost, N., van de Giesen, N., van Werkhoven, B., Abdollahi, B., Aerts, J., Albers, T., Alidoost, F., Andela, B., Camphuijsen, J., Dzigan, Y., van Haren, R., Hutton, E., Kalverla, P., van Meersbergen, M., van den Oord, G., Pelupessy, I., Smeets, S., Verhoeven, S., de Vos, M., and Weel, B.: The eWaterCycle platform for open and FAIR hydrological collaboration, *Geosci. Model Dev.*, 15, 5371-5390, 10.5194/gmd-15-5371-2022, 2022.
- Ivanov, V. Y., Vivoni, E. R., Bras, R. L., and Entekhabi, D.: Catchment hydrologic response with a fully distributed triangulated irregular network model, *Water Resour Res*, 40, <https://doi.org/10.1029/2004WR003218>, 2004.
- Jones, J. E. and Woodward, C. S.: Newton-Krylov-multigrid solvers for large-scale, highly heterogeneous, variably saturated flow problems, *Adv Water Resour*, 24, 763-774, Doi 10.1016/S0309-1708(00)00075-0, 2001.
- Keune, J., Gasper, F., Goergen, K., Hense, A., Shrestha, P., Sulis, M., and Kollet, S.: Studying the influence of groundwater representations on land surface-atmosphere feedbacks during the European heat wave in 2003, *J Geophys Res-Atmos*, 121, 13301-13325, 10.1002/2016jd025426, 2016.
- Kollet, S., Sulis, M., Maxwell, R. M., Paniconi, C., Putti, M., Bertoldi, G., Coon, E. T., Cordano, E., Endrizzi, S., Kikinzon, E., Mouche, E., Mügler, C., Park, Y.-J., Refsgaard, J. C., Stisen, S., and Sudicky, E.: The integrated hydrologic model intercomparison project, IH-MIP2: A second set of benchmark results to diagnose integrated hydrology and feedbacks, *Water Resour Res*, 53, 867-890, <https://doi.org/10.1002/2016WR019191>, 2017.
- Kollet, S. J. and Maxwell, R. M.: Integrated surface-groundwater flow modeling: A free-surface overland flow boundary condition in a parallel groundwater flow model, *Adv Water Resour*, 29, 945-958, 2006.
- Kollet, S. J. and Maxwell, R. M.: Capturing the influence of groundwater dynamics on land surface processes using an integrated, distributed watershed model, *Water Resour Res*, 44, Artn W0240210.1029/2007wr006004, 2008.
- Kumar, S. V., Reichle, R. H., Peters-Lidard, C. D., Koster, R. D., Zhan, X., Crow, W. T., Eylander, J. B., and Houser, P. R.: A land surface data assimilation framework using the land information system: Description and applications, *Adv Water Resour*, 31, 1419-1432, <https://doi.org/10.1016/j.advwatres.2008.01.013>, 2008.
- Kurtz, W., He, G., Kollet, S. J., Maxwell, R. M., Vereecken, H., and Hendricks Franssen, H. J.: TerrSysMP-PDAF (version 1.0): a modular high-performance data assimilation framework for an integrated land surface-subsurface model, *Geosci. Model Dev.*, 9, 1341-1360, 10.5194/gmd-9-1341-2016, 2016.
- Lawrence, D. M., Fisher, R. A., Koven, C. D., Oleson, K. W., Swenson, S. C., Bonan, G., Collier, N., Ghimire, B., van Kampenhout, L., Kennedy, D., Kluzek, E., Lawrence, P. J., Li, F., Li, H., Lombardozzi, D., Riley, W. J., Sacks, W. J., Shi, M., Vertenstein, M., Wieder, W. R., Xu, C., Ali, A. A., Badger, A. M., Bisht, G., van den Broeke, M., Brunke, M. A., Burns, S. P., Buzan, J., Clark, M., Craig, A., Dahlin, K., Drewniak, B., Fisher, J. B., Flanner, M., Fox, A. M., Gentine, P., Hoffman, F., Keppel-Aleks, G., Knox, R., Kumar, S., Lenaerts, J., Leung, L. R., Lipscomb, W. H., Lu, Y., Pandey, A., Pelletier, J. D., Perket, J., Randerson, J. T., Ricciuto, D. M., Sanderson, B. M., Slater, A., Subin, Z. M., Tang, J., Thomas, R. Q., Val Martin, M., and Zeng, X.: The Community Land Model Version 5: Description of New Features, Benchmarking, and Impact of Forcing Uncertainty, *J Adv Model Earth Sy*, 11, 4245-4287, <https://doi.org/10.1029/2018MS001583>, 2019.
- Leung, L. R., Bader, D. C., Taylor, M. A., and McCoy, R. B.: An Introduction to the E3SM Special Collection: Goals, Science Drivers, Development, and Analysis, *J Adv Model Earth Sy*, 12, e2019MS001821, <https://doi.org/10.1029/2019MS001821>, 2020.
- Liu, J., Yang, Z.-L., Jia, B., Wang, L., Wang, P., Xie, Z., and Shi, C.: Elucidating Dominant Factors Affecting Land Surface Hydrological Simulations of the Community Land Model over China, *Advances in Atmospheric Sciences*, 40, 235-250, 10.1007/s00376-022-2091-5, 2023.
- Mackay, D. S., Roberts, D. E., Ewers, B. E., Sperry, J. S., McDowell, N. G., and Pockman, W. T.: Interdependence of chronic hydraulic dysfunction and canopy processes can improve integrated models of tree response to drought, *Water Resour Res*, 51, 6156-6176, <https://doi.org/10.1002/2015WR017244>, 2015.
- Maina, F. Z., Rosen, D., Abbaszadeh, P., Yang, C., Kumar, S. V., Rodell, M., and Maxwell, R.: Integrating the Interconnections Between Groundwater and Land Surface Processes Through the Coupled NASA Land Information System and ParFlow Environment, *J Adv Model Earth Sy*, 17, e2024MS004415, <https://doi.org/10.1029/2024MS004415>, 2025.





- Maxwell, R. M.: A terrain-following grid transform and preconditioner for parallel, large-scale, integrated hydrologic modeling, *Adv Water Resour*, 53, 109-117, <https://doi.org/10.1016/j.advwatres.2012.10.001>, 2013.
- Maxwell, R. M. and Condon, L. E.: Connections between groundwater flow and transpiration partitioning, *Science*, 353, 377-380, 2016.
- Maxwell, R. M. and Miller, N. L.: Development of a coupled land surface and groundwater model, *J Hydrometeorol*, 6, 233-247, 2005.
- Maxwell, R. M., Chow, F. K., and Kollet, S. J.: The groundwater–land–surface–atmosphere connection: Soil moisture effects on the atmospheric boundary layer in fully-coupled simulations, *Adv Water Resour*, 30, 2447-2466, <https://doi.org/10.1016/j.advwatres.2007.05.018>, 2007.
- Maxwell, R. M., Condon, L. E., and Kollet, S. J.: A high-resolution simulation of groundwater and surface water over most of the continental US with the integrated hydrologic model ParFlow v3, *Geosci Model Dev*, 8, 923-937, 10.5194/gmd-8-923-2015, 2015.
- Maxwell, R. M., Lundquist, J. K., Mirocha, J. D., Smith, S. G., Woodward, C. S., and Tompson, A. F. B.: Development of a Coupled Groundwater-Atmosphere Model, *Mon Weather Rev*, 139, 96-116, 10.1175/2010mwr3392.1, 2011.
- Maxwell, R. M., Putti, M., Meyerhoff, S., Delfs, J.-O., Ferguson, I. M., Ivanov, V., Kim, J., Kolditz, O., Kollet, S. J., Kumar, M., Lopez, S., Niu, J., Paniconi, C., Park, Y.-J., Phanikumar, M. S., Shen, C., Sudicky, E. A., and Sulis, M.: Surface-subsurface model intercomparison: A first set of benchmark results to diagnose integrated hydrology and feedbacks, *Water Resour Res*, 50, 1531-1549, <https://doi.org/10.1002/2013WR013725>, 2014.
- Mikkelsen, K. M., Maxwell, R. M., Ferguson, I., Stednick, J. D., McCray, J. E., and Sharp, J. O.: Mountain pine beetle infestation impacts: modeling water and energy budgets at the hill-slope scale, *Ecohydrology*, 6, 64-72, <https://doi.org/10.1002/eco.278>, 2013.
- Muñoz-Sabater, J., Dutra, E., Agustí-Panareda, A., Albergel, C., Arduini, G., Balsamo, G., Boussetta, S., Choulga, M., Harrigan, S., Hersbach, H., Martens, B., Miralles, D. G., Piles, M., Rodríguez-Fernández, N. J., Zsoter, E., Buontempo, C., and Thépaut, J. N.: ERA5-Land: a state-of-the-art global reanalysis dataset for land applications, *Earth Syst. Sci. Data*, 13, 4349-4383, 10.5194/essd-13-4349-2021, 2021.
- Niu, G.-Y., Paniconi, C., Troch, P. A., Scott, R. L., Durcik, M., Zeng, X., Huxman, T., and Goodrich, D. C.: An integrated modelling framework of catchment-scale ecohydrological processes: 1. Model description and tests over an energy-limited watershed, *Ecohydrology*, 7, 427-439, <https://doi.org/10.1002/eco.1362>, 2014.
- Niu, G.-Y., Yang, Z.-L., Mitchell, K. E., Chen, F., Ek, M. B., Barlage, M., Kumar, A., Manning, K., Niyogi, D., Rosero, E., Tewari, M., and Xia, Y.: The community Noah land surface model with multiparameterization options (Noah-MP): 1. Model description and evaluation with local-scale measurements, *Journal of Geophysical Research: Atmospheres*, 116, <https://doi.org/10.1029/2010JD015139>, 2011.
- O'Neill, M. M. F., Tijerina, D. T., Condon, L. E., and Maxwell, R. M.: Assessment of the ParFlow–CLM CONUS 1.0 integrated hydrologic model: evaluation of hyper-resolution water balance components across the contiguous United States, *Geosci. Model Dev.*, 14, 7223-7254, 10.5194/gmd-14-7223-2021, 2021.
- Oleson, K. W., Niu, G. Y., Yang, Z. L., Lawrence, D. M., Thornton, P. E., Lawrence, P. J., Stöckli, R., Dickinson, R. E., Bonan, G. B., Levis, S., Dai, A., and Qian, T.: Improvements to the Community Land Model and their impact on the hydrological cycle, *Journal of Geophysical Research: Biogeosciences*, 113, <https://doi.org/10.1029/2007JG000563>, 2008.
- Osei-Kuffuor, D., Maxwell, R. M., and Woodward, C. S.: Improved numerical solvers for implicit coupling of subsurface and overland flow, *Adv Water Resour*, 74, 185-195, <https://doi.org/10.1016/j.advwatres.2014.09.006>, 2014.
- Poll, S., Rigor, P., van Hulten, M., Patakchi Yousefi, K., Cavedes Voullieme, D., Goergen, K., and Kollet, S. J.: The new version of the Terrestrial Systems Modeling Platform (TSMP2) based on ICON, eCLM, and ParFlow, *AGU Fall Meeting Abstracts*, A32F-01,
- Rahman, M., Sulis, M., and Kollet, S. J.: The subsurface-land surface-atmosphere connection under convective conditions, *Adv Water Resour*, 83, 240-249, 10.1016/j.advwatres.2015.06.003, 2015.
- Raupach, M. R.: Drag and drag partition on rough surfaces, *Boundary-Layer Meteorology*, 60, 375-395, 10.1007/BF00155203, 1992.





- Raupach, M. R.: Simplified expressions for vegetation roughness length and zero-plane displacement as functions of canopy height and area index, *Boundary-Layer Meteorology*, 71, 211-216, 10.1007/BF00709229, 1994.
- Reinecke, R., Foglia, L., Mehl, S., Trautmann, T., Cáceres, D., and Döll, P.: Challenges in developing a global gradient-based groundwater model (G3M v1.0) for the integration into a global hydrological model, *Geosci. Model Dev.*, 12, 2401-2418, 10.5194/gmd-12-2401-2019, 2019.
- Rihani, J. F., Chow, F. K., and Maxwell, R. M.: Isolating effects of terrain and soil moisture heterogeneity on the atmospheric boundary layer: Idealized simulations to diagnose land-atmosphere feedbacks, *J Adv Model Earth Sy*, 7, 915-937, <https://doi.org/10.1002/2014MS000371>, 2015.
- Rihani, J. F., Maxwell, R. M., and Chow, F. K.: Coupling groundwater and land surface processes: Idealized simulations to identify effects of terrain and subsurface heterogeneity on land surface energy fluxes, *Water Resour Res*, 46, 2010.
- Scanlon, B. R., Zhang, Z., Save, H., Sun, A. Y., Müller Schmied, H., van Beek, L. P. H., Wiese, D. N., Wada, Y., Long, D., Reedy, R. C., Longuevergne, L., Döll, P., and Bierkens, M. F. P.: Global models underestimate large decadal declining and rising water storage trends relative to GRACE satellite data, *Proceedings of the National Academy of Sciences*, 115, E1080-E1089, doi:10.1073/pnas.1704665115, 2018.
- Seuffert, G., Gross, P., Simmer, C., and Wood, E. F.: The Influence of Hydrologic Modeling on the Predicted Local Weather: Two-Way Coupling of a Mesoscale Weather Prediction Model and a Land Surface Hydrologic Model, *J Hydrometeorol*, 3, 505-523, [https://doi.org/10.1175/1525-7541\(2002\)003<0505:TIOHMO>2.0.CO;2](https://doi.org/10.1175/1525-7541(2002)003<0505:TIOHMO>2.0.CO;2), 2002.
- Shangguan, W., Dai, Y., Duan, Q., Liu, B., and Yuan, H.: A global soil data set for earth system modeling, *J Adv Model Earth Sy*, 6, 249-263, 10.1002/2013ms000293, 2014.
- Shrestha, P., Sulis, M., Masbou, M., Kollet, S., and Simmer, C.: A Scale-Consistent Terrestrial Systems Modeling Platform Based on COSMO, CLM, and ParFlow, *Mon Weather Rev*, 142, 3466-3483, <https://doi.org/10.1175/MWR-D-14-00029.1>, 2014.
- Skamarock, W. C. and Klemp, J. B.: A time-split nonhydrostatic atmospheric model for weather research and forecasting applications, *Journal of Computational Physics*, 227, 3465-3485, <https://doi.org/10.1016/j.jcp.2007.01.037>, 2008.
- Smith, S., Ferguson, I., Engdahl, N., Gasper, F., Chennault, C., Triana, J. S. A., Avery, P., Rigor, P., Condon, L., Jourdain, S., Bennett, A., Artavanis, G., Maxwell, R., Kulkarni, K., Bansal, V., Beisman, J., de Rooij, R., Swilley, J., Lazzeri, D., Thompson, D., Coon, E., Bertolacci, I., Azeemi, M. F., Wagner, N.: parflow/parflow: ParFlow Version 3.13.0 (v3.13.0), Zenodo [code], <https://doi.org/10.5281/zenodo.10989198>, 2024.
- Sulis, M., Meyerhoff, S. B., Paniconi, C., Maxwell, R. M., Putti, M., and Kollet, S. J.: A comparison of two physics-based numerical models for simulating surface water-groundwater interactions, *Adv Water Resour*, 33, 456-467, <https://doi.org/10.1016/j.advwatres.2010.01.010>, 2010.
- Sulis, M., Williams, J. L., Shrestha, P., Diederich, M., Simmer, C., Kollet, S. J., and Maxwell, R. M.: Coupling Groundwater, Vegetation, and Atmospheric Processes: A Comparison of Two Integrated Models, *J Hydrometeorol*, 18, 1489-1511, <https://doi.org/10.1175/JHM-D-16-0159.1>, 2017.
- Tai, X., Mackay, D. S., Sperry, J. S., Brooks, P., Anderegg, W. R. L., Flanagan, L. B., Rood, S. B., and Hopkinson, C.: Distributed Plant Hydraulic and Hydrological Modeling to Understand the Susceptibility of Riparian Woodland Trees to Drought-Induced Mortality, *Water Resour Res*, 54, 4901-4915, <https://doi.org/10.1029/2018WR022801>, 2018.
- Tran, H., Leonarduzzi, E., De la Fuente, L., Hull, R. B., Bansal, V., Chennault, C., Gentile, P., Melchior, P., Condon, L. E., and Maxwell, R. M.: Development of a Deep Learning Emulator for a Distributed Groundwater&ndash;Surface Water Model: ParFlow-ML, *Water*, 13, 3393, 2021.
- Valcke, S.: Highlights from a Workshop on the Latest Updates on Coupling Technologies and Coupled Applications in Earth System Modeling, *B Am Meteorol Soc*, 103, E657-E664, <https://doi.org/10.1175/BAMS-D-21-0045.1>, 2022.
- van den Hurk, B., Kim, H., Krinner, G., Seneviratne, S. I., Derksen, C., Oki, T., Douville, H., Colin, J., Ducharme, A., Cheruy, F., Viovy, N., Puma, M. J., Wada, Y., Li, W., Jia, B., Alessandri, A., Lawrence, D. M., Weedon, G. P., Ellis, R., Hagemann, S., Mao, J., Flanner, M. G., Zampieri, M., Matera, S., Law, R. M., and Sheffield, J.: LS3MIP (v1.0) contribution to CMIP6: the Land Surface, Snow and Soil moisture Model Intercomparison Project – aims,



- 848 setup and expected outcome, *Geosci. Model Dev.*, 9, 2809-2832, 10.5194/gmd-9-2809-  
 849 2016, 2016.
- 850 Verkaik, J., Sutanudjaja, E. H., Oude Essink, G. H. P., Lin, H. X., and Bierkens, M. F. P.:  
 851 GLOBGM v1.0: a parallel implementation of a 30 arcsec PCR-GLOBWB-MODFLOW  
 852 global-scale groundwater model, *Geosci. Model Dev. Discuss.*, 2022, 1-27, 10.5194/gmd-  
 853 2022-226, 2022.
- 854 Williams, J. L. and Maxwell, R. M.: Propagating Subsurface Uncertainty to the Atmosphere  
 855 Using Fully Coupled Stochastic Simulations, *J Hydrometeorol*, 12, 690-701,  
 856 <https://doi.org/10.1175/2011JHM1363.1>, 2011.
- 857 Xue, M., Droegemeier, K. K., and Wong, V.: The Advanced Regional Prediction System (ARPS)  
 858 – A multi-scale nonhydrostatic atmospheric simulation and prediction model. Part I: Model  
 859 dynamics and verification, *Meteorol Atmos Phys*, 75, 161-193, 10.1007/s007030070003,  
 860 2000.
- 861 Xue, M., Droegemeier, K. K., Wong, V., Shapiro, A., Brewster, K., Carr, F., Weber, D., Liu, Y.,  
 862 and Wang, D.: The Advanced Regional Prediction System (ARPS) – A multi-scale  
 863 nonhydrostatic atmospheric simulation and prediction tool. Part II: Model physics and  
 864 applications, *Meteorol Atmos Phys*, 76, 143-165, 10.1007/s007030170027, 2001.
- 865 Yang, C.: ParFlow-CoLM, Zenodo [code], <https://doi.org/10.5281/zenodo.16879407>, 2025.
- 866 Yang, C., Maxwell, R., McDonnell, J., Yang, X., and Tijerina-Kreuzer, D.: The Role of  
 867 Topography in Controlling Evapotranspiration Age, *Journal of Geophysical Research:*  
 868 *Atmospheres*, 128, e2023JD039228, <https://doi.org/10.1029/2023JD039228>, 2023.
- 869 Yang, C., Jia, Z., Xu, W., Wei, Z., Zhang, X., Zou, Y., McDonnell, J., Condon, L., Dai, Y., and  
 870 Maxwell, R.: CONCN: a high-resolution, integrated surface water–groundwater ParFlow  
 871 modeling platform of continental China, *Hydrol. Earth Syst. Sci.*, 29, 2201-2218,  
 872 10.5194/hess-29-2201-2025, 2025.
- 873 Yang, C., Li, H.-Y., Fang, Y., Cui, C., Wang, T., Zheng, C., Leung, L. R., Maxwell, R. M., Zhang,  
 874 Y.-K., and Yang, X.: Effects of Groundwater Pumping on Ground Surface Temperature: A  
 875 Regional Modeling Study in the North China Plain, *Journal of Geophysical Research:*  
 876 *Atmospheres*, 125, e2019JD031764, 10.1029/2019jd031764, 2020.
- 877 Yeh, P. J. F. and Eltahir, E. A. B.: Representation of Water Table Dynamics in a Land Surface  
 878 Scheme. Part I: Model Development, *J Climate*, 18, 1861-1880,  
 879 <https://doi.org/10.1175/JCLI3330.1>, 2005.
- 880 York, J. P., Person, M., Gutowski, W. J., and Winter, T. C.: Putting aquifers into atmospheric  
 881 simulation models: an example from the Mill Creek Watershed, northeastern Kansas, *Adv*  
 882 *Water Resour*, 25, 221-238, [https://doi.org/10.1016/S0309-1708\(01\)00021-5](https://doi.org/10.1016/S0309-1708(01)00021-5), 2002.
- 883 Yuan, H. and Dai, Y.: Description of the Common Land Model (CoLM 2024), Sun Yat-sen  
 884 University Press, Guangzhou, China, 2025.
- 885 Yuan, H., Dickinson, R. E., Dai, Y., Shaikh, M. J., Zhou, L., Shangguan, W., and Ji, D.: A 3D  
 886 Canopy Radiative Transfer Model for Global Climate Modeling: Description, Validation, and  
 887 Application, *J Climate*, 27, 1168-1192, <https://doi.org/10.1175/JCLI-D-13-00155.1>, 2014.
- 888 Yuan, H., Dai, Y., Dickinson, R. E., Pinty, B., Shangguan, W., Zhang, S., Wang, L., and Zhu,  
 889 S.: Reexamination and further development of two-stream canopy radiative transfer models  
 890 for global land modeling, *J Adv Model Earth Sy*, 9, 113-129,  
 891 <https://doi.org/10.1002/2016MS000773>, 2017.
- 892 Zeng, Y. J., Xie, Z. H., Liu, S., Xie, J. B., Jia, B. H., Qin, P. H., and Gao, J. Q.: Global Land  
 893 Surface Modeling Including Lateral Groundwater Flow, *J Adv Model Earth Sy*, 10, 1882-  
 894 1900, 10.1029/2018ms001304, 2018.
- 895